PREDICTION OF CRACK GROWTH IN BRIDGE ROLLER BEARINGS

Nawal K. Prinja[1], Joseph M. Bushell[1], Ramesh Chandwani[2] and Chris Timbrell[2]

[1]AMEC Nuclear UK Ltd

[2]Zentech International Ltd

THEME

Failure prediction and assessment.

KEYWORDS

Crack Growth, Roller Bearing, Failure Investigation, Abaqus, Zencrack

SUMMARY

This paper explains how the general purpose FE code Abaqus was combined with Zencrack to predict 3D crack growth as part of an investigation conducted to explain failure of single cylinder bridge roller bearings. Finite Element analyses were conducted to gain an understanding of the stresses caused during operation and explain the possible cause of crack growth resulting in failure. It was important to predict sub-surface crack growth in the rollers induced by repeated rolling as the bridge expands due to daily and seasonal temperature cycles. Models of the bearings were required to represent the contact between the roller and plates, daily movement of the load and the non-linear behaviour of the material. A band of pressure due to contact with the plates traverses back and forth over the roller as it rotates. The ambient temperature changes were such that the roller would experience at least one stress cycle per day of operation.

A number of initial crack scenarios are studied, based on crack initiation sites identified during inspections of the failed rollers. Stress intensity factors (SIFs) for all three modes of cracking (K_I, K_{II} and K_{III}) are plotted against angle of roll for these analyses to help explain the crack growth and resulting failure. If the

bearing is misaligned, the roller is subjected to additional twist. The Abaqus and Zencrack analyses showed that in the absence of any twist, the load cycling caused by the rotation of the roller propagates initial end cracks along the roller axis which can lead to the roller splitting in half. Twisting of the roller due to bearing misalignment causes out of plane growth of the crack indicating that a part of the roller can break away.

1: INTRODUCTION

The analysis presented concerns an investigation into failures of single cylinder roller bearings used to support the Thelwall viaduct on the M6 motorway in the UK. The bearings were designed to permit thermal expansion of the bridge deck due to daily and seasonal temperature cycles. A number of bearings were found to have cracked within 3 years of installation. Nearly 25% of the bearings were found to have suffered significant cracking with many others showing indications of crack initiation.

An illustration of a typical roller bearing is shown in Figure 1. Metallurgical investigations of the failed rollers showed cracks to have initiated from the end faces of the rollers, a few millimetres below the contact surface with the plates.

The stainless steel AISI 420 TQ+T material used for manufacturing such bearings is prone to small surface cracks due to intergranular attack (IGA). Under cyclic loading these cracks can be sufficiently large to grow, leading to gross structural failure. Finite Element Analysis (FEA) combined with 3D crack growth studies were carried out as part of the failure investigation to explain the likely failure mechanism.

This paper describes the analyses conducted to gain an understanding of the stresses caused during operation and provides an explanation of the possible cause of crack growth resulting in failure. It was important to predict sub-surface crack growth in the rollers induced by repeated rolling under high contact loads.

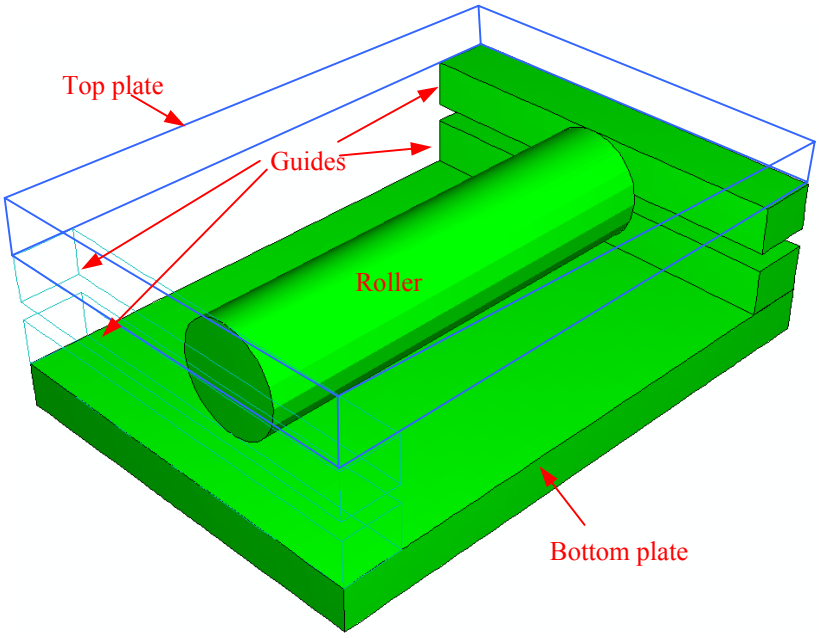

Figure 1: Simplified illustration of a typical Thelwall Viaduct roller bearing.

2: FE MODEL AND CRACK GROWTH ANALYSIS

The roller selected for analysis has a diameter of 120mm and a length of 480mm. Rolling analyses were undertaken to investigate the growth of initial cracks at one end of the roller under the following conditions:

a) Perfectly aligned bearing

b) Misaligned bearings with the application of end load on the roller due to contact with the guides

c) Small scale crack growth of IGA initiated crack around roller with chamfered end

For brevity, results are presented for analysis of conditions (a) and (c) only.

Analyses were undertaken using the crack propagation software Zencrack [1] and Abaqus/Standard [2]. Zencrack is used to insert a postulated crack into an existing uncracked FE mesh of the roller bearing and following analysis in Abaqus determines both crack growth magnitude and direction at individual points along the crack front. Progressive crack front development under continued cyclic loading is predicted by calculation of a new crack position and update of the FE mesh. The interaction between these software packages to allow crack growth prediction is summarised in the flowchart presented in Figure 2.

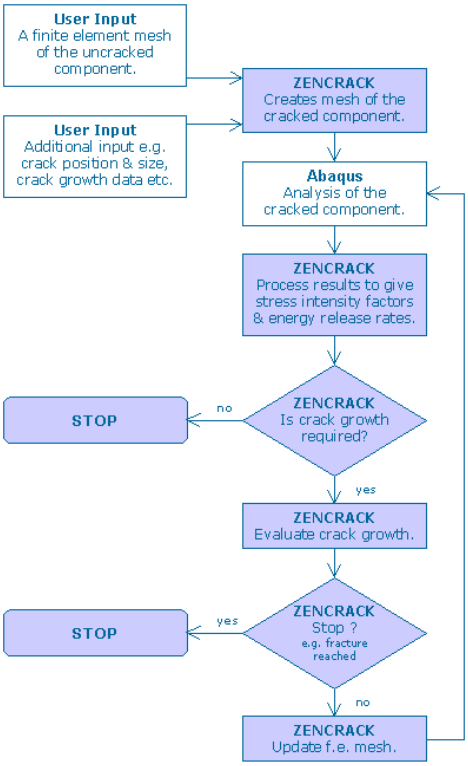

Figure 2: Flowchart showing the interaction between Zencrack and Abaqus.

3: ANALYSIS OF THE PERFECTLY ALIGNED ROLLER

The purpose of this analysis was to predict the growth of cracks beginning at the end face of the roller and at the edge of the contact zone where cracks had been observed to initiate.

In this analysis, the bearing is assumed to be perfectly aligned with no contact between the roller end faces and the guides. The uncracked roller mesh prior to insertion of cracks by Zencrack is shown in Figure 3. Four large 20-noded elements are defined as targets for replacement by Zencrack's "crack-blocks". This allows modelling of the two initial corner cracks of 10mm radius and scope for analysis of a fully through crack. The target elements in the uncracked mesh must be 20-noded elements to allow definition of the curved outer surface of the roller. A section through the resulting initial cracked mesh is shown in Figure 4. The inserted elements of the crack-blocks are 8 noded bricks (C3D8) which are tied to the surrounding mesh region (also C3D8 elements) using the Abaqus surface-based tying option, *TIE. Mesh sensitivity was checked by doubling the number of elements. The crack-block region extends 150mm axially into the roller. The circumferential extent of the crack-blocks is such that contact between the roller and top and bottom plates does not extend out of the crack-block region. The plates are modelled as rigid

surfaces. The bottom plate is fixed and the top plate given a vertical load followed by horizontal translation. At zero degrees role, the cracks are directly beneath the line of contact between the roller and plates. The top plate was translated ±27mm, giving a roll of approximately ±12.9 degrees. The roller is linear elastic with E=205500MPa and ν=0.3. All analyses have the Abaqus option of NLGEOM=YES to apply the large-displacement formulation to account for the geometric and contact non-linearities associated with the analysis. Sensitivity to friction between the crack faces was also assessed by analysing the crack growth under the same load case with values of friction of 0 and 0.8.

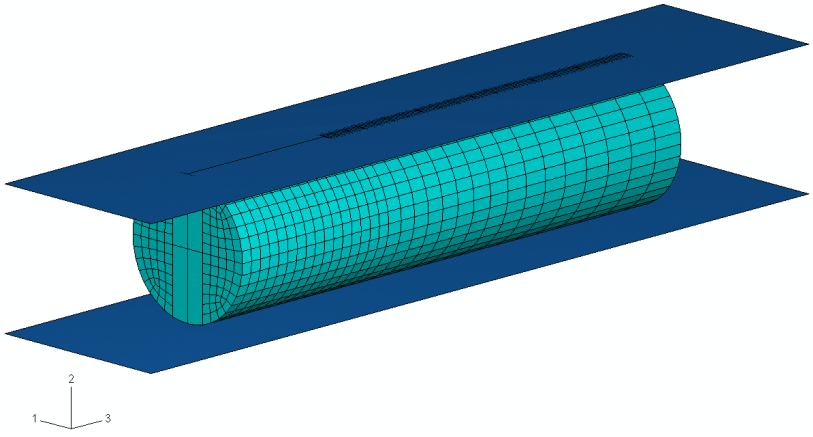

Figure 3: Model with uncracked mesh and crack block region.

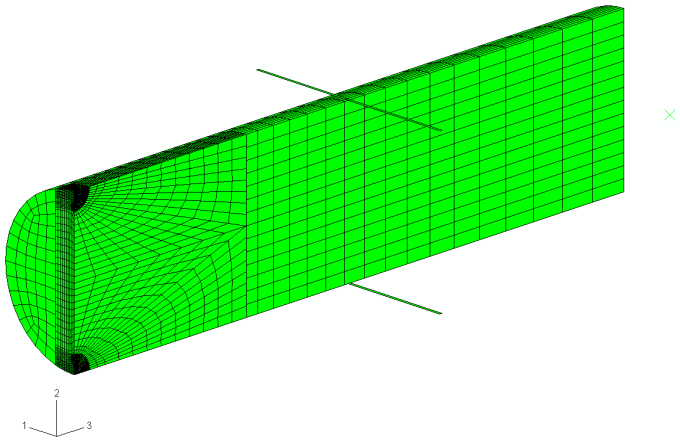

Figure 4: Mesh with initial crack.

Crack Growth Law

The following crack growth law is applied in the analysis. Shear (Mode II) cracking is considered the dominant mode for size of crack considered, therefore the magnitude of crack growth is determined by evaluating ΔK_{II}.

$$\frac{da}{dN} = \frac{\pi}{90\sigma_f{}^2} \frac{\Delta K_{II}{}^4}{\left(K_{IIC}{}^2 - K_{II}{}^2\right)} \quad (1)$$

where σ_f is the flow stress of the material. Zencrack evaluates growth direction by calculating the direction of maximum energy release at each node along the crack front, taking into account contributions from Modes I (tensile), II (in-plane shear) and III (out-of-plane shear) cracking.

Fracture Behaviour

Stress intensity factors (SIFs) were monitored at two crack front locations identified in Figure 5. SIFs are plotted for Modes I, II and III against angle of roll for each location in Figures 6 and 7 respectively for a 10mm corner crack. Due to symmetry both crack fronts behave in the same fashion.

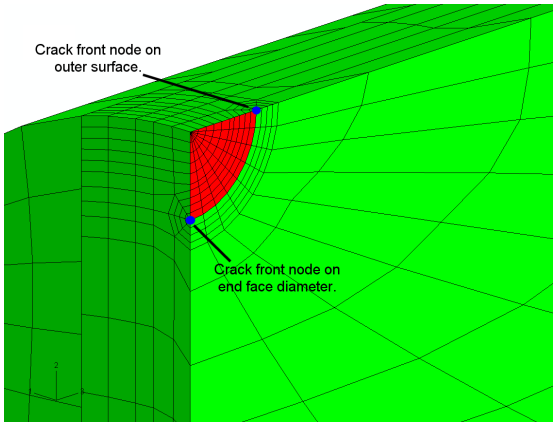

Figure 5: Node positions on the 10mm corner crack front for SIF plots

At zero degrees roll there is a narrow band of closure along the contact region between the roller and plate. This is reflected in the plots of K_I in Figure 6 which show values of zero for the 'outer surface' node position at and near zero degrees roll. The crack faces in this region begin to open slightly as roll increases and K_I begins to rise. The K_I remains small, however, compared to the peak value at the 'end face' node position shown in Figure 6 (around 30 MPamm^{½} and 50 MPamm^{½} for the outer surface node compared to peaks of 350 MPamm^{½}and 450 MPamm^{½} at the end face node). At the end face node position on the diameter, the crack is open at zero degrees roll giving a peak K_I value for this position. As the roll angle increases the relative opening of the crack faces decreases across the majority of the crack face. For a small crack size this effect is more pronounced and at maximum roll the crack face is virtually fully closed. As it begins to grow, the crack retains a small region of crack face that is open, even at maximum roll. The K_I value at the end face node position decreases to zero at about 5 degrees roll.

The behaviour of K_{III} at the outer surface node position and K_{II} at the end face node position both dominate their respective K_{II} and K_{III} counterparts. This is as a result of the main vertical load acting to influence K_{III} at the outer surface node and K_{II} at the end face node. At zero roll the outer surface node cannot develop any relative tearing due to the constraint provided by the plate. Hence K_{III} is zero. As the roll angle increases, the vertical load acts on one side of the crack and significant K_{III} develops at this point. At the end face node position on the diameter, the zero roll position prevents shearing opening and hence K_{II} is zero. As the roll begins, there is significant relative shearing motion at the end face node position and hence K_{II} increases significantly. Although they also play a part, the K_{II} effect at the outer surface node position and the K_{III} effect at the end face node position are less important and peak values reach only around 50% of the respective K_{III} and K_{II} values.

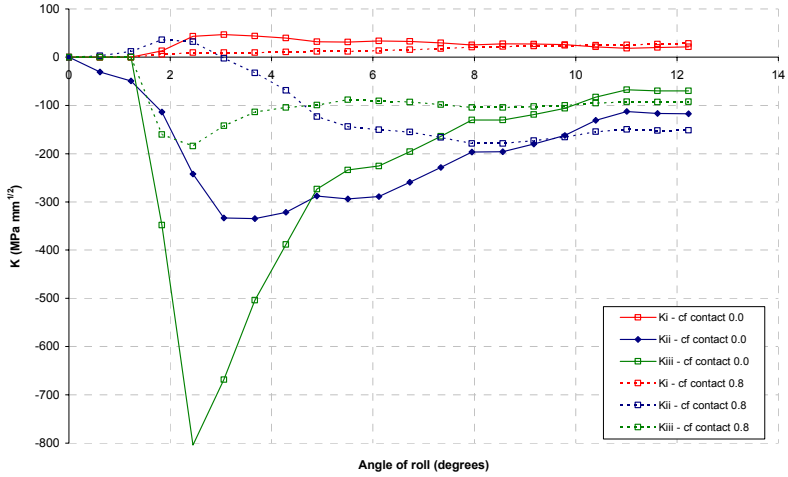

Figure 6: Variation of K_I, K_{II} and K_{III} on the "outer surface" crack front position for the 10mm corner crack

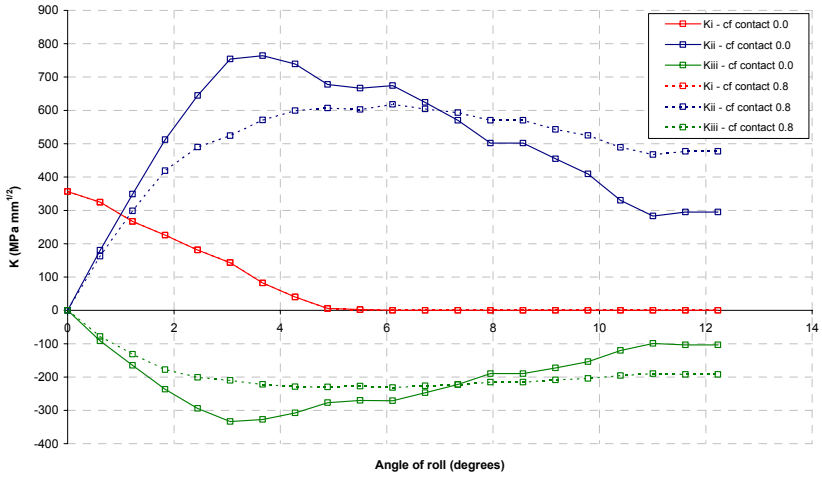

Figure 7: Variation of K_I, K_{II} and K_{III} on the "end face" crack front position for the 10mm corner crack

For the K_{II} and K_{III} at each node position on the crack face studied, the peak occurs at a roll angle of around 3 degrees with a steady decrease for additional roll. Notably, this brings the location of the crack tip at the outer surface of the roller to just outside the area of contact between the roller and plate (found from separate nonlinear studies of roller to be 2-3mm either side of centre). This indicates that only about 3 degrees of rolling is sufficient to reach peak stress intensity and the roller experience the maximum possible damage. In addition, Figures 6 and 7 show the variation in K for zero to $+12.9^{o}$ roll. When considering a full cycle of positive and negative roll about the zero position, K_{II} and K_{III} will reach equal and opposite peaks at +3 and -3 degrees, giving ΔK_{II} and ΔK_{III} of twice the range shown in Figures 6 and 7. Damage due to these components is clearly significant during a typical rolling cycle.

The effect on the outer surface node of adding friction between the crack faces is to significantly reduce K_I, K_{II} and K_{III}, indicating that crack growth local to the contact area would be noticeably reduced. For the end diameter node position, K_{II} and K_{III} are also reduced as these modes rely on relative sliding of the crack faces against one another, although to a lesser extent. K_I is unaffected as in this mode the crack faces are separated.

Crack Growth Prediction

The crack growth analysis was conducted to determine the pattern of growth of the two initial corner cracks under repeated horizontal cycling of the top plate. The predicted crack growth profiles are shown in Figure 8 and compared with those observed on a typical failed roller where growth of two cracks initiated at one end of the roller resulted in splitting the roller in half. The analysis is carried out in two stages. Firstly, simultaneous growth of the two corner cracks is modelled with repeated cycling until a transition point is reached where the cracks coalesce into a through crack phase. The initial through crack profile is based on the final corner crack positions. At the transition from corner to through crack, the crack extends 92mm axially long the roller outer surface. Beyond this transition point, the central region of the crack is observed to grow quickly compared to the upper and lower regions. The predicted crack growth profiles are remarkably similar to those observed from the beachmarks on the roller, as shown in Figure 8. This analysis terminates when the crack growth law fails i.e. K_{IIC} is exceeded in the denominator of the crack growth law defined earlier (1). At this point the crack has straightened out and the average axial crack length is 107.1mm. A significant increase in crack growth rate was observed when end loads due to top plate misalignment were added to the analysis.

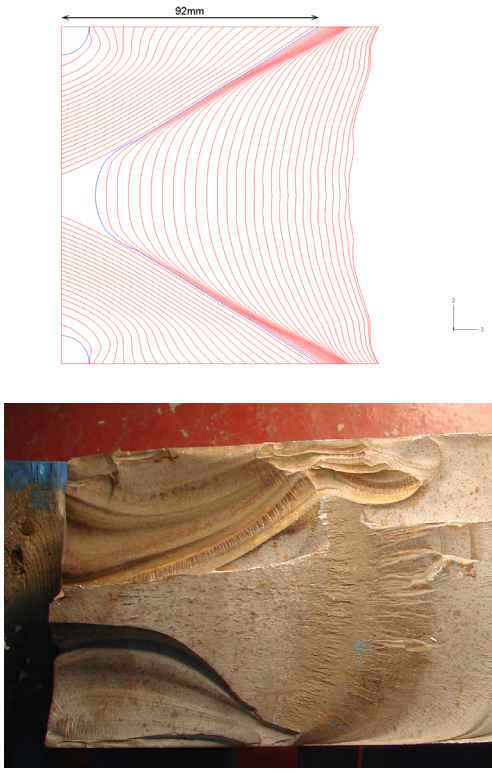

Figure 8: Predicted and observed crack growth in a roller with two initial corner cracks

4: SMALL SCALE CRACK GROWTH OF IGA-INITIATED CRACK

Geometry, crack definition and loading

The analysis of the 'perfect' roller studied crack growth from a semi-circular defect encompassing the end edge of the roller. A further study was performed to determine whether it would be possible for an inter-granular crack at the observed initiation site on the roller end faces would propagate under the action of load cycling due to rolling.

Figure 9 shows the location and geometry of the crack considered. The crack is a shallow, elliptical shape, 3mm in length with a depth typical of the inter-granular corrosion observed on the surface of the rollers (300μm). Separate detailed nonlinear FEA of the uncracked rollers revealed a localised hotspot of tensile hoop stress at this location, approximately 4mm beneath the line of contact, that diminished rapidly in magnitude with depth into the roller. It was postulated that this tensile stress could provide a driver towards initial development of the crack. Following this initial period of development, further crack growth would be driven by the significant shear modes identified in the analysis previously presented in Section 3.

As small scale growth of the crack is now considered, the chamfer around the edge between the roller end face and contact surface is now explicitly modelled.

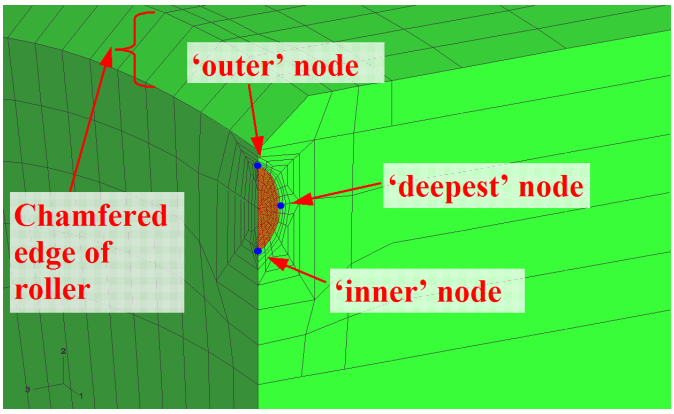

Figure 9: Initial inter-granular crack analysed for crack growth

Crack Growth Law

The crack growth law applied in the study of the perfect roller (1) assumed Mode II dominance in the crack growth law. This was an appropriate assumption for the large scale crack growth mechanism observed. Preliminary analyses showed that, at the scale of the inter-granular crack, all three modes provided similar contributions to the overall crack growth. The crack growth law was therefore modified to ensure that whatever the dominant mode at a point along the crack front, the maximum amount of growth would be captured.

$$\frac{da}{dN} = \frac{\pi}{90\sigma_f{}^2}\left[\frac{\Delta K_I{}^4}{\left(K_{IC}{}^2 - K_I{}^2\right)} + \frac{\Delta K_{II}{}^4}{\left(K_{IIC}{}^2 - K_{II}{}^2\right)} + \frac{\Delta K_I{}^4}{\left(K_{IIIC}{}^2 - K_{III}{}^2\right)}\right] \quad (2)$$

Analysis Results

Figures 10, 11 and 12 show the variation in K_I, K_{II} and K_{III} for each of the crack positions shown in Figure 9. Similar characteristics are demonstrated by this crack to the larger crack in the 'perfect' roller analysis, in that K_I reaches its peak at zero degrees roll when the crack is directly beneath the contact line, and K_{II} and K_{III} peak at a few degrees roll about centre. However, the magnitudes are much smaller, due to the general smaller crack size and that the chamfer shields the crack from the full action of the load applied by the plate.

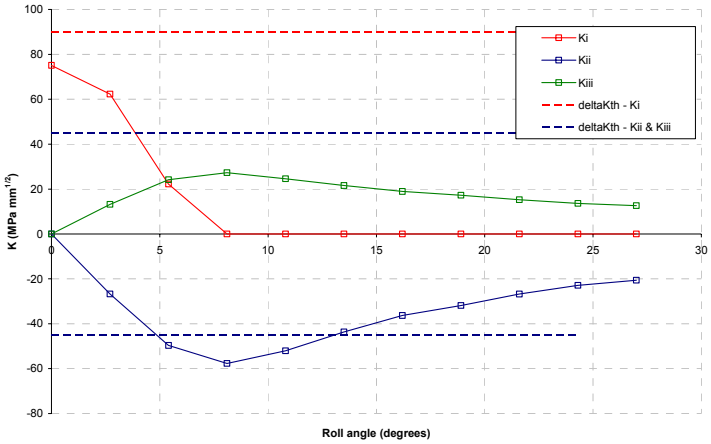

Figure 10: Variation of K_I, K_{II} and K_{III} on the "inner" crack front position for the "IGA" initial crack size

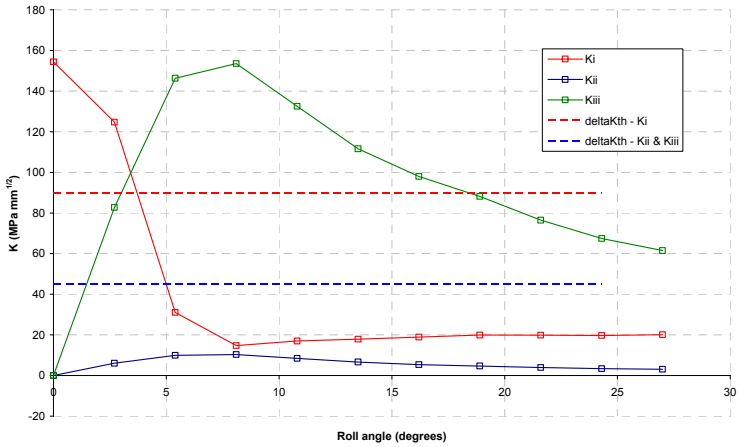

Figure 11: Variation of K_I, K_{II} and K_{III} on the "deepest" crack front position for the "IGA" initial crack size

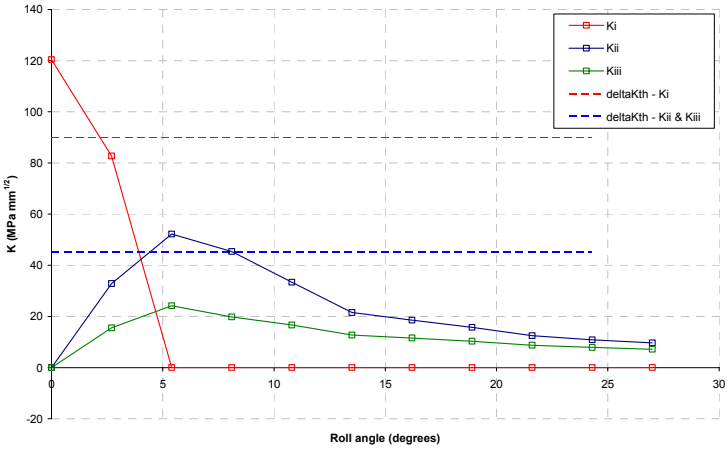

Figure 12: Variation of K_I, K_{II} and K_{III} on the "outer" crack front position for the "IGA" initial crack size

Considering a typical threshold stress intensity range for this material of 90 MPa $mm^{1/2}$ (45 MPa $mm^{1/2}$ for K_{II} and K_{III} which will reverse during a full rolling cycle), this suggests that only slow growth will initially occur at the very edges of the crack. However, K_I and K_{II} at the deepest node clearly exceed threshold, as shown in Figure 11, allowing the crack to initially 'burrow' into the roller. The increase in crack size eventually pulls the stress intensity values at the outer edges of the crack well above threshold to allow further growth to occur. The resulting crack profile is shown in Figure 13. Growth is initially slower at this scale compared to the larger scale growth modelled, but this shows that even a small crack may propagate under cyclic load. Other environmental factors, such as corrosion, that are not considered in this analysis may also influence the rate of crack growth.

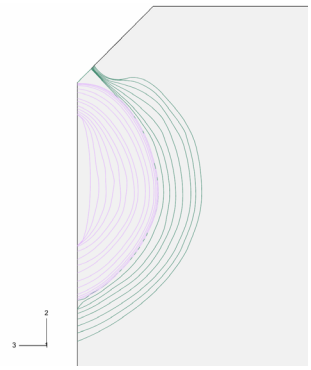

Figure 13: Predicted growth of 'IGA' crack under cyclic load

5: CONCLUSIONS

This numerical investigation has offered an insight into the failure mechanisms of a bridge bearing roller subjected to a linear load which induces cyclic loads as the roller rolls back and forth. The analyses have demonstrated that initial imperfections, which may exist due to IGA, may propagate as the line of high local compression traverses the surface of the roller. Initial small scale growth of the IGA initiator is driven by a combination of Mode I, II and III crack growth. Once the crack has reached a sufficient size, the main drivers for large scale crack growth are shear modes II and III. Qualitative and quantitative agreement has been demonstrated with the observed crack patterns.

6: REFERENCES

1. Zencrack 7.4 development version, Zentech International Ltd., http://www.zentech.co.uk

2. Abaqus/Standard 6.5-1, Abaqus Inc, Providence, RI, USA